Article

Few-Layer Graphene from Mechanical Exfoliation of Graphite-Based Materials: Structure-Dependent Characteristics

Azhar A. Pirzado [1,2]**, François Le Normand** [2]**, Thierry Romero** [1]**, Sandra Paszkiewicz** [3] **,
Vasiliki Papaefthimiou** [1]**, Dris Ihiawakrim** [4] **and Izabela Janowska** [1,*]

[1] Institut de Chimie et Procédés pour l'Énergie, l'Environnement et la Santé (ICPEES), CNRS UMR 7515-University of Strasbourg, 25 rue Becquerel, 67087 Strasbourg, France; pirzado@etu.unistra.fr (A.A.P.); thierry.romero@unistra.fr (T.R.); papaefthymiou@unistra.fr (V.P.)

[2] Laboratoire des sciences de l'Ingénieur, de l'Informatique et de l'Imagerie (ICube), UMR 7357, CNRS – University of Strasbourg, 67400 Strasbourg, France; francois.le-normand@unistra.fr

[3] West Pomeranian University of Technology, Institute of Material Science and Engineering Piastow Av. 19, 70310 Szczecin, Poland; spaszkiewicz@zut.edu.pl

[4] Institut de Physique et Chimie des Matériaux de Strasbourg (IPCMS), CNRS UMR 7504-University of Strasbourg, France; drisihi@ipcms.unistra.fr

* Correspondence: janowskai@unistra.fr; Tel.: +33-(0)36-885-2633

check for updates

Abstract: We present a high-scale method to produce few-layer graphene (FLG) based on the mechanical exfoliation of graphite and compare the obtained FLG with the one reported earlier arising from pencil lead ablation. Several elements were modified and improved in the new approach. The purification and the ablation set-up were simplified, and the morphology of the FLG was modified and improved in view of some applications. The morphology-dependent properties of FLGs, lead-FLG, and graphite-FLG as conductive layers and in nanocomposites were investigated. The newly obtained FLG had a higher aspect ratio (high lateral size vs thickness/higher 2D aspect), which is reflected by enhanced transparency–conductivity features of the layer (film) and elongation-at-break behavior of the polymer composites. On the contrary, the nanocomposite containing lead-FLG showed, for instance, excellent gas barrier properties due to the multi-step structure of the lead-FLG flakes. Such structure exhibited less 2D and more 3D character, which can be highly suitable for applications where the presence of active/reactive edges is beneficial, e.g., in catalysis or supercapacitors' electrodes. Nuclear reaction analysis was employed to investigate the morphology of graphite-FLG film.

Keywords: few-layer graphene; mechanical exfoliation; graphene nanocomposites; conductive layer; nuclear reaction analysis

1. Introduction

A significant number of methods have been developed for the production of graphene and/or few-layer graphene (FLG), since graphene was mechanically isolated from graphite by a scotch tape for the first time in 2004 [1]. The ideal method should fit the envisaged applications in terms of cost, efficiency, and scalability, but also the morphological properties of the obtained FLG product. High expectations from the industry concerning the applications of graphene and graphene-based materials also induce a permanent search for efficient methods that additionally could answer the sustainable development requirements. Bottom-up methods such as catalytic chemical vapor deposition (CVD) or epitaxial growth over SiC produce high-quality graphene films dedicated to more sophisticated needs in electronics, optoelectronics, spintronics, and related fields [2,3], while their limited yields

and scalability exclude them from many other applications. The fields that require high-yield "bulk graphene"/FLG powder/platelets are, for instance, high-performance composites, conductive inks, coatings, and catalysis. They focus on top-down approaches dealing with the exfoliation of graphite-based materials where the van der Waals forces between sheets in the graphite need to be defeated. The most common top-down method is the ultrasonication-assisted exfoliation in liquids, either in an organic solvent with the appropriate surface tension [4] or in aqua solution in the presence of surfactant. Additionally, a large number of works reporting the production of reduced graphene oxide focus mostly on the restoration of the continuous conjugated –C=C– lattice lost during the highly oxidative exfoliation of graphite into graphite oxide [5]. The recent prominent exfoliation in water instead involves the use of bio-surfactants [6,7], where high exfoliation yield and highly concentrated colloids can be reached [7]. Apart from exfoliation improvement by chemistry, the mechanically applied shear forces and the way they are applied play a significant role, impacting the efficiency and structure of the resulting FLG. A significant progress in FLG production was observed, for instance, when a kitchen blender [8], microfluidization [9], or mixing-assisted ultrasonication were applied [7].

The scarce top-down methods concern the mechanical exfoliation of graphite, including the scotch tape approach, and usually either proceed with low yield or lead to FLG with a highly disturbed morphology, as is the case for ball-milled graphite [1,10,11]. One of the highest yield methods reported by us a few years ago is the mechanical ablation of a pencil lead on a rough glass surface [12]. The ablation was assisted by the simultaneous ultrasonication of the glass surface in ethanol (water) aiming at the detachment of the ablated (exfoliated) products.

Herein, we show several beneficial modifications of this mechanical ablation method that were conducted by replacing the pencil lead by graphite discs with an adaptation of the processing and set-up.

2. Materials and Methods

Lead-FLG was obtained according to the work reported previously [12].

Graphite-FLG was obtained through the mechanical ablation of a pure graphite disc (provided by Nanocyl) on a rough glass surface. The set-up consisted of a modified polishing-like apparatus, in which the horizontal glass disc, as the ablation substrate, turned with a controlled speed, while the graphite disc hung loosely over the glass surface, kept by a suction cup system from the top. A stream of ethanol was systematically used to remove the material ablated and attached to the glass surface. Next, the product of the ethanol suspension was submitted to a sedimentation process for 4 h. The supernatant containing FLG was then separated with an overall yield of around 60% and dried under vacuum evaporation. Eventually, a final drying in a standard oven at 100 °C for 2 h was applied.

FLG layers/films were prepared from ethanol suspensions with concentrations of 0.5 mg/mL that were sprayed on preheated and continuously heated quartz plates at 120 °C with Airgun (Hi-line Iwata). Air was used as a carrier gas with gun inlet pressure of 1.5 bars.

Thermal annealing of the films was performed at 900 °C for 2 h under Ar flow.

Transmission electron microscopy (TEM) was carried out on a Topcon 002B-UHR microscope working with an accelerated voltage of 200 kV and a point-to-point resolution of 0.17 nm. The sample was dispersed in ethanol, and a drop of the suspension was deposited onto a carbon-coated copper grid for analysis. In the case of composites, a slice of composite was cut prior to analysis.

Scanning electron microscopy (SEM) analysis was carried out on a JEOL 6700-FEG microscope.

Thermogravimetric analyses (TGA) were carried out on a TA instrument SDT Q600 under air; the rate of heating was fixed at 5°/min.

Raman spectroscopy was performed using a Horiba Scientific Labram Aramis Raman Spectrometer (Jobin Yvon technology) with the following conditions: laser wavelength of 532.15 nm, D2 filter (1% power) and spectrum in regions from 1250 to 1650 cm^{-1} and from 2600 to 2800 cm^{-1}, with integration time of 100 s for each phase.

The X-ray Photoelectron Spectroscopy (XPS) measurements were performed in an ultrahigh vacuum (UHV) setup equipped with a VSW ClassWA hemispherical electron analyzer with a multi-channeltron detector. A monochromated AlKα X-ray source (1486.6 eV; anode operating at 240 W) was used as incident radiation. The base chamber pressure was 1×10^{-9} mbar. High-resolution spectra were recorded in constant-pass-energy mode (100 and 20 eV, respectively). Prior to individual elemental scans, a survey scan was taken for all the samples, to detect all of the present elements.

Ultraviolet Photoelectron spectroscopy (UPS) measurements. During the work function measurements by UPS ($h\nu$ = 21.2 eV), a bias of 15.31 V was applied to the samples in order to avoid interference of the spectrometer threshold in the UP spectra. The work function of the surface was determined from the UP spectra by subtracting their width (i.e., the energy difference between the Fermi level and the high binding energy cutoff) from the He I excitation energy (21.2 eV).

Transmission spectra (UV–Vis) were obtained on a VARIAN Cary 100 Scan UV–Visible spectrometer which had a deuterium arc and tungsten halogen lamps.

The thickness of the graphite–FLG was measured by a Veeco DEKTAK 150 profilometer.

Four-point probes (FPPs) measurements were performed in order to achieve sheet resistance (R_s) of the lead–FLG and graphite–FLG films using Keithley 220 programmable current source coupled with a Hewlett-Packard 34401A multimeter. For some films, a pair of electrodes (Au/Cr) was deposited. It was, however, noticed by the systemically performed measurements that the electrodes were not necessary to maintain good contact with the FLG films, and the measurable values were comparable with those of electrode-free films.

The average thickness of the films was measured by a Dektac a (and confirmed by atomic force microscopy).

Nuclear reaction analysis (NRA). The ion beam analysis was carried out on a 4MV Van De Graff accelerator facility, using deuterium (2H) as an incident ion with energy of 900 keV and a scattering angle of 150°. The conversion from channel (C) to energy (E) in keV (arbitrary number slots converted to corresponding energy values, E = 7.04 $\times$ C − 85.00) was done by using the standard oxygen and carbon nuclear reactions [O^{16}(d,p_0)O^{17}], [O^{16} (d,p_1)O^{17}] and [C^{12}(d,p)C^{13}]. The bare SiO_2 and SiC samples were used for the calibration of the spectra. The spectra were calibrated by using SiO_2 and SiC samples for oxygen and carbon, using the standard oxygen and carbon nuclear reactions [O^{16}(d,p_0)O^{17}], [O^{16} (d,p_1)O^{17}] and [C^{12}(d,p)C^{13}]. The spectra were fitted with the SIMRA software.

3. Results and Discussion

3.1. Ablation Process/FLG Structure

For the present purpose, the discs of two kinds of graphite were used for the mechanical ablation: highly oriented pyrolytic graphite (HOPG) and thermal pyrolytic graphite (TPG).

According to the previous general procedure of mechanical exfoliation, the graphite disc is ablated on a rough glass surface using an automatic set-up, while the ablated (exfoliated) product is detached from the surface using a stream of solvent (ethanol or possibly water) [12]. The ablation set-up is, however, modified compared to the one used for pencil lead (see Methods). Figure 1 is a draft representing the ablations of both pencil lead and graphite disc. The presence of an inorganic binder, such as kaolin in pencil lead, was not the only difference between the lead and graphite disc. It was that the final products, FLG flakes, varied in terms of morphology, more precisely, by the size and flakes' edges. The FLG flakes from the exfoliation of lead often demonstrated a "multi-step" structure (Figures 1a and 2a), which was previously confirmed by TEM and through the stabilization of metal nanoparticles (NPs) [13] also in the self-assembling process where "3D-like particle" behavior was observed [14]. A multi-step structure was also present in the edges but was observed less frequently in the case of FLG originating from the graphite discs. We ascribe this difference to a different arrangement of the initial graphite species in the lead versus the graphite disc. The surface of ablation was parallel to the macroscopic surface of the graphitic disc but usually not parallel to the graphitic moieties in

the lead. In the latter, the graphitic species were relatively smaller and randomly arranged under a different angle, as they were spaced by the inorganic binder.
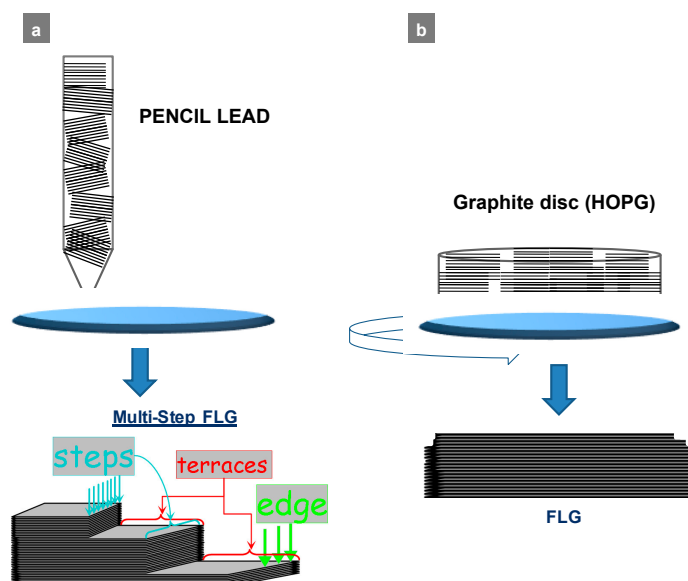

Figure 1. Draft of the ablation process over a rough glass surface (**a**) of a pencil lead and (**b**) of a graphite disc; related few-layer graphene (FLG) morphologies (lead-FLG with highly multi-step structure vs graphite-FLG).
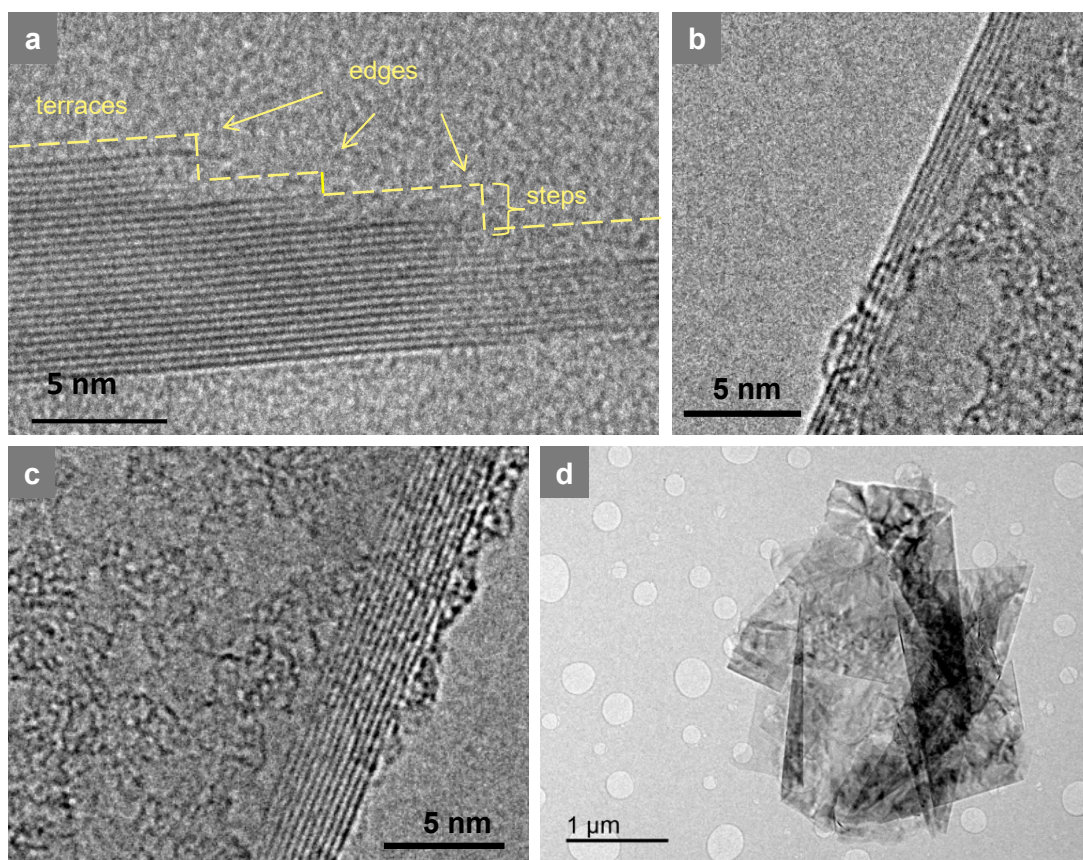

Figure 2. Transmission electron microscopy (TEM) micrographs of (**a**) a thicker flake of lead-FLG with multi-step structure, (**b** and **c**) variable number of sheets in graphite-FLG from the supernatant and settled-down part, respectively, and (**d**) overall view of the assembly of graphite-FLG flakes.

Figure 2 shows the related TEM micrographs of the edges of FLGs exfoliated from both precursors, where, additionally, the number of layers can be counted. In a similar way to the pencil lead ablation, the ablation of graphite was followed by a step of sedimentation, which aimed to separate the heavily exfoliated part of graphite. Likewise, the final supernatant (after a few hours of sedimentation) contained FLG flakes with a number of sheets rarely exceeding 10, while the settled-down part was multi-layer graphene (MLG) with a number of sheets up to 40. Unlike FLG from a pencil lead, no purification treatment was required in the case of graphite-FLG, since no inorganic binder was present. The overall yield of graphite-FLG product reached around 60%–70%. The solvent, in this case ethanol, could then be removed, for instance, by a standard rotary evaporator (Figure 3a), without inducing excessive stacking of the flakes. We find it important to highlight this simple and fast step, since no literature reports such evaporation for graphene-based materials. This kind of evaporation would seem to favor the π–π stacking between the FLG sheets; however, it can be stopped before the solvent is totally removed leaving a thin layer of solvent adsorbed on the FLG surface (due to the low pressure, the applied drying temperature can be highly decreased as well compared to standard drying). The remaining layer, in this case ethanol, helped the dispersion of FLG afterwards in polar solvents, as required for the introduction of FLG into polymers.
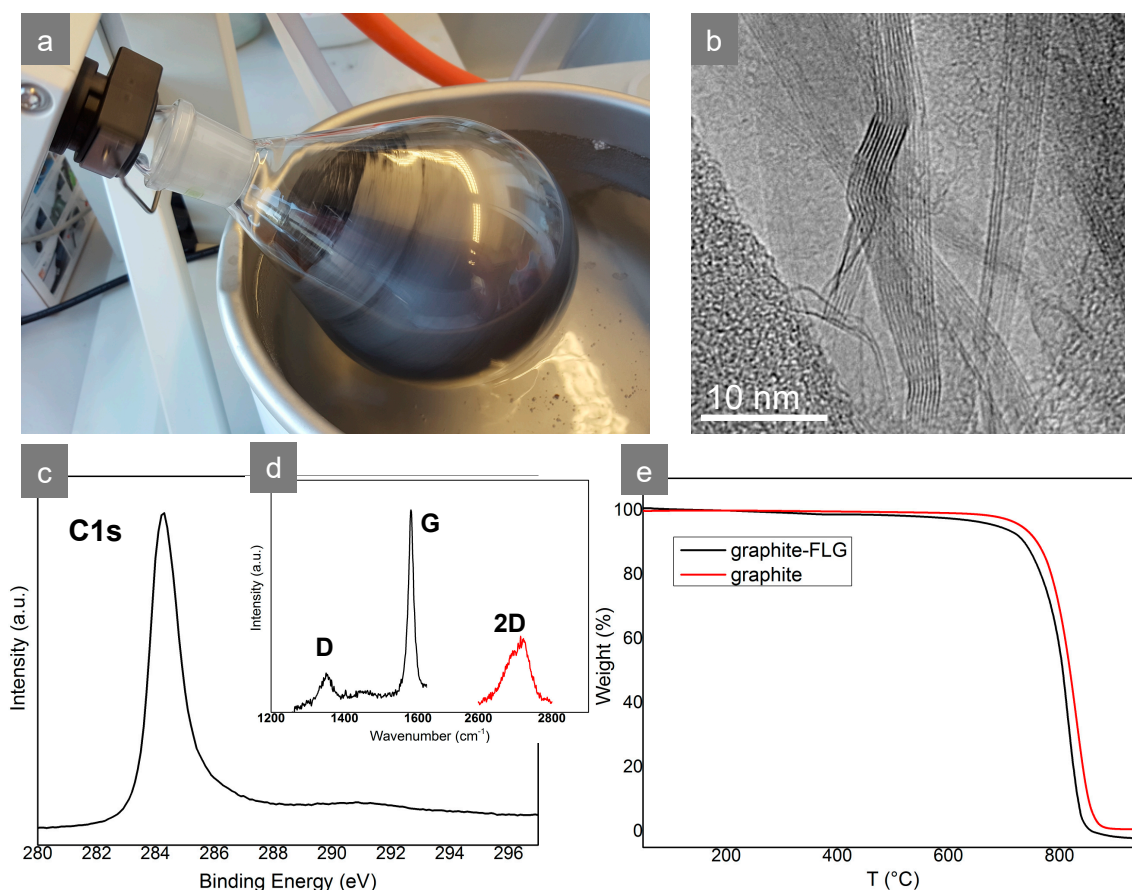

Figure 3. (**a**) Removal of the solvent from the FLG suspension by rotary evaporation, (**b**) TEM micrograph of graphite-FLG embedded into a polymer (PTF) showing different number of edges/sheets in particular FLG flakes (3–9 sheets), (**c**) C1s XPS spectrum of graphite-FLG, (**d**) Raman spectrum of graphite-FLG, and (**e**) TGA curves of graphite and graphite-FLG.

The high purity of the graphite-FLG product was confirmed by XPS, Raman, and TGA analyses (Figure 3 c–e). As it can be seen, the thin and relatively symmetric C1s peak at ca. 284.5 eV in the XPS spectrum revealed a high content of sp^2 carbon and a very low content of sp^3 carbon and oxygen-bonded C, whose signatures appeared at higher binding energy, above 285 up to ca. 290 eV.

On the contrary, a clear π–π* transition loss peak at 291 eV revealing easy electron delocalization could be observed [15]. The low ratio of relative D and G peaks' intensity I_D/I_G = 0.13 in Raman spectra confirmed a very high content of undisturbed conjugated cyclic carbon. The shape of the 2D peak in selected flakes at c.a. 2700 cm^{-1} suggests few, but no more than five, layers in the analyzed flake (the intensity of the broad part of the peak at lower wavelength is significant) [16]. Likewise, graphite-FLG oxidized at a relatively high temperature (under air), around 700 °C, while, as expected, it started to be oxidized 30–40 °C earlier than graphite before the ablation.

3.2. FLG in Nanocomposites

The rotary-assisted-evaporated graphite-FLG was used next as an additive filler with 0.1 and 0.3 wt % in poly(trimethylene 2,5-furanoate) (PTF), where very high dispersion of FLG was observed after nanocomposite formation using an in situ polymerization process. The polymerization was preceded by dispersing the FLG in the monomer [17]. It was found that the addition of 0.3% of FLG (PTF–FLG) did not increase the electrical conductivity. It slightly decreased oxygen transmission, while thermal conductivity and elongation at break were significantly improved.

For a nanocomposite based on poly(trimethylene tetraphtalate) containing FLG from ablation of lead (PTT–FLG), different effects were observed. Here, for the same FLG content (0.3%), the elongation at break was strongly decreased (ε_b[%] is 2.28 vs. 178.32 for pure PTT), while, on the contrary, the permeability behavior was excellent, and the O_2 and CO_2 transmission of PTT–FLG dropped to negligible values, from 74.3 to 2.3 and from 649.6 to 36.7 cm^3/m^2 × 24h, respectively.

Although the two polymers (PTF, PTT) are different and the interactions between them and FLG may vary, the signature of FLG morphology in the two composites was clear and suggested a higher aspect ratio (lateral size vs thickness) of FLG originating from pure graphite. The significant aspect ratio should indeed provide a higher elongation at break and possibly create some preferential 2D paths of percolation in the graphite-FLG composite. Locally, the PTT was less charged with FLG, which permitted, however, gas passing (nanocomposite films of 5 cm^2 were subjected to permeability measurements). On the contrary, the lower size and edges-rich lead-FLG was highly and more homogenously distributed in the nanocomposite, and its multi-step structures with inequivalent edges (and so inequivalent graphitic planes) helped to inhibit the permeability of gases at higher overall volume (surface and thickness), similar to a cascade-like barrier.

3.3. FLG Conductive Layer/Film/Electrode

The higher lateral size of the graphite-FLG flakes and structure homogeneity could be observed by SEM (Figure 4a,b) and also by investigation of the transparency–conductivity trade-off in FLG films (Figure 4d–f) [18]. The FLG films/layers were formed by deposition of both FLGs over transparent substrates via the hot-spray technique, followed by annealing treatment in Ar. The annealing process allowed the removal of ethanol and other possible impurities adsorbed on the FLG flakes' surface, which resulted in a decrease of the resistance. Both FLGs were deposited in minimum, but high enough, quantity to obtain a conductive layer. The layer formed from graphite-FLG showed a transparency up to 74% for a same range of conductivity (Rs ≈ 21 kΩ/sq) compared to FLG from the lead (Rs ≈ 15 kΩ/sq), whose transparency did not exceed 35%. It is worthy to note that conductivity measurements were done by the FPPs method. The Hall Effect method measurements performed previously (under N_2) for lead-FLG showed lower Rs by one order of magnitude, 1 kΩ/sq [19]. These results show that the charge transport properties were more hindered in the case of lead-FLG compared to graphite-FLG: this was due firstly to the lower aspect ratio and, secondly, to the multi-step structure of the former. The conductivity of the films were calculated to be σ = 3.7 S/cm and 5.1 S/cm for graphite-FLG and lead-FLG, respectively, while, considering the transparency–conductivity figure of merit, the calculated "conductivity of transparency" values were σ_{gt} = 61 S/cm and 41 S/cm for graphite-FLG and lead-FLG, respectively [18].
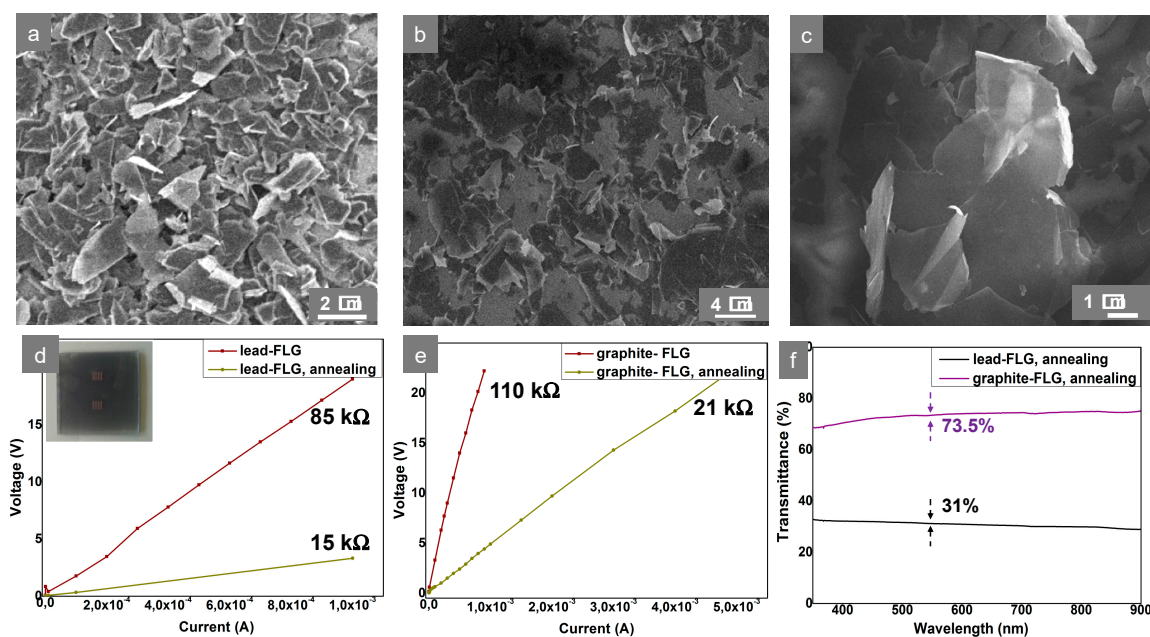
Figure 4. (**a**–**c**) Scanning electron microscopy (SEM) micrographs of sprayed layers: (**a**) Lead-FLG, (**b**,**c**) graphite-FLG; (**d**,**e**) I–V curves obtained by the four-point probes (FPPs) method for lead- and graphite-FLG layers (without and after annealing), respectively, and (**f**) transmittance curves of lead- and graphite-FLG layers, for comparable conductivities of the films (Rs = 15kΩ/sq and 21 kΩ/sq, respectively).

The higher aspect ratio and, more precisely, the high lateral size of graphite-FLG flakes allowed percolation and transport through the macroscopic surface (in 2D) at lower surface coverage. This entailed the higher overall transparency.

In order to get more information about the morphology of the graphite-FLG layer prepared by hot spray, the thickness of the film was measured by profilometry, and the volume density (carbon) was determined afterwards by Nuclear Reaction Analysis (NRA). We find it interesting to highlight at this point the use of NRA, since NRA is rarely applied for analysis of such relatively thick films prepared by high-scale methods such as spraying. Figure 5a displays the NRA spectra obtained for a conductive graphite-FLG film with ^{12}C (d, p)^{13} signal at ca. 2735 keV [20].
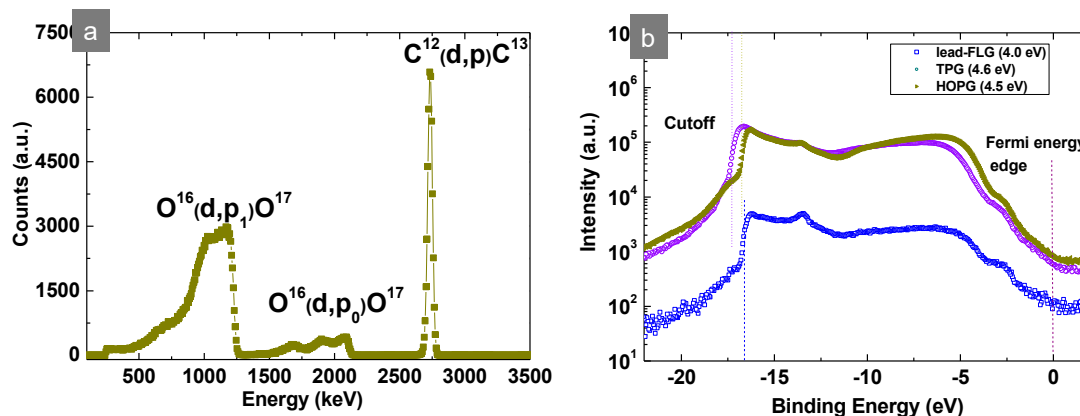

Figure 5. (**a**) Nuclear Reaction Analysis (NRA) spectra obtained for the graphite-FLG film (electrode) with carbon ^{12}C at 2770 keV and (**b**) UPS work functions of lead- and graphite-FLG samples.

Because of the resolution of NRA analysis (up to a few μm), the depth profile included the FLG film and SiO$_2$ substrate displaying two oxygen peaks for the two reactions. It was calculated from

SIMRA software that the cross-sectional surface density (A) contained 6.25×10^{17} atoms/cm^2, while the average thickness of the film (T_f) was 130 nm according to the profilometer measurements. On the basis of these two values, the volume density of the FLG film (ρ_f) could be calculated according to Equation (1):

$$\rho_f = A \times M/(N_A \times T_f) = 6.25 \times 10^{17} \times 12/(130 \times 10^{-7} \times 6.023 \times 10^{23}) = 0.96 \text{ g/cm}^3 \qquad (1)$$

where N_A is the Avogadro number (6.023×10^{23} atoms/mol), and *M* is the molecular weight of carbon (12 g/mol).

The obtained volume density of the FLG film, ρ_f, was much lower than the volume density of graphite (~2.25 g/cm^3), indicating that more than half of the volume of the FLG film was void (~57%).

Despite a significant amount of voids, the FLG film was conductive, meaning that the amount and arrangement of the FLG flakes were sufficient to form conductive paths. On the other hand, regarding the average thickness of the film and amount of voids, it is important to note that the overall transparency of the film was also due to the voids and not only to the low thickness of the FLG flakes themselves. The transmittance values obtained by UV–Vis spectroscopy were measured for micrometric spots that covered a relatively high surface, including the FLG flakes and the voids. The low homogeneity and still relatively low transparency of such prepared FLG film make it insufficient for applications like transparent conductive films/electrodes (TCFs). However, conductive layers/film with other useful properties such as hydrophobicity, anti-static properties, thermal conductivity, etc. can be easily obtained. Yet, further optimization of the FLG-graphite structure by additional separation methods and appropriate deposition would lead to better transparency–conductivity–homogeneity characteristics of the films. Meanwhile, in view of the potential application of mechanically ablated FLGs as electrodes/conductive layers, work functions (Φ) measurements were additionally performed by the UPS method. The Φ values were determined by subtracting the difference between the UPS secondary cutoff (cutoff) and Fermi edges E$_f$. The obtained Φ for lead-FLG, 4.0 $\pm$ 0.1 eV, was much lower than the Φ of graphite/graphene, ~ 4.6 eV [21], which could be related to the purification step and the structure itself. The Φ of TPG-FLG and HOPG-FLG, 4.6 $\pm$ 0.1 and 4.5 $\pm$ 0.1 eV, respectively, corresponded to Φ of graphite/graphene and were almost equivalent to Φ of ITO (4.7 eV), showing that this FLG could be envisaged for applications in optoelectronics if, of course, the conductivity/transparency trade-off is resolved. On the contrary, the FLG-lead will be more appropriate as an electrode with a low Φ, for instance as a solution-processable material that can replace metal-based counter electrodes (cathodes) in organic photovoltaic (OPV) cells (Ag, Al electrode: 4.0–4.3 eV). The metal electrodes are in general deposited by costly evaporation methods such as sputtering.

4. Conclusions

The significant modifications of morphology and some related properties of FLG obtained by the mechanical ablation (exfoliation) of graphite were compared to those of FLG obtained previously by ablation of pencil lead. The new approach is a high-yield and simple method with a simplified set-up and absence of additional purification steps. The new product (graphite-FLG) consists of flakes of few/several sheets with much higher aspect ratio and more homogenous structure compared to lead-FLG. Because of the different arrangement and purity of graphitic entities in the initial materials, larger FLG flakes with homogenous size of sheets and equivalent edges were obtained, while multi-step-structure FLG flakes from pencil lead were often observed. The two different structures of graphite-FLG and lead-FLG reflect different signatures in nanocomposites (in polymers) and in conductive layers. The enhanced conductivity–transparency properties of film and increased elongation at break in nanocomposites of graphite-FLG compared to lead-FLG were measured. In turn, the increased number of effective edges in the multi-step FLG flakes (lead-FLG) is advantageous for the reduction of gases permeability in nanocomposites but also, e.g., for the enhancement of dispersion

and stabilization of metal nanoparticles for catalytic applications. NRA analysis of the graphite-FLG films was used to get inside cross-sectional density and porosity of the film, and UPS analysis was used to check the work function values for both graphite- and lead-FLG. The work function also varied for both types of FLG, placing them in different potential electrode applications. Concerning the lower aspect ratio and multi-step structure of lead-FLG flakes, they exhibited less 2D and more 3D character, which can be highly suitable for applications where the presence of active/reactive edges is beneficial, e.g., in catalysis [22] or supercapacitors' electrodes [23].

References

1. Novoselov, K.S.; Geim, A.K.; Morozov, S.V.; Jiang, D.; Zhang, Y.; Dubonos, S.V.; Grigorieva, I.V.; Firsov, A.A. Electric Field Effect in Atomically Thin Carbon Films. *Science* **2004**, *306*, 666–669. [CrossRef]

2. Zhang, Y.; Zhang, L.; Zhou, C. Review of Chemical Vapor Deposition of Graphene and Related Applications. *Acc. Chem. Res.* **2013**, *46*, 2329–2339. [CrossRef] [PubMed]

3. Mishra, N.; Boeckl, J.; Motta, N.; Iacopi, F. Graphene growth on silicon carbide: A review. *Phys. Status Solidi* **2016**, *2013*, 2277–2289. [CrossRef]

4. Hernandez, Y.; Nicolosi, V.; Lotya, M.; Blighe, F.M.; Sun, Z.; De, S.; McGovern, I.T.; Holland, B.; Byrne, M.; Gun'Ko, Y.K.; et al. High- yield production of graphene by liquid-phase exfoliation of graphite. *Nat. Nanotechnol.* **2008**, *3*, 563–568. [CrossRef]

5. Rozada, R.; Paredes, J.I.; Villar-Rodil, S.; Martínez-Alonso, A.; Tascón, J.M.D. Towards full repair of defects in reduced graphene oxide films by two-step graphitization. *Nano Res.* **2013**, *6*, 216–233. [CrossRef]

6. Paredes, J.I.; Villar-Rodil, S. Biomolecule-assisted exfoliation and dispersion of graphene and other two-dimensional materials: a review of recent progress and applications. *Nanoscale* **2016**, *8*, 15389–15413. [CrossRef] [PubMed]

7. Ba, H.; Truong-Phuoc, L.; Pham-Huu, C.; Luo, W.; Baaziz, W.; Romero, T.; Janowska, I. Colloid Approach to the Sustainable Top-Down Synthesis of Layered Materials. *ACS Omega* **2017**, *2*, 8610–8617. [CrossRef]

8. Yi, M.; Shen, Z. Kitchen blender for producing high-quality few-layer graphene. *Carbon* **2014**, *78*, 622–626. [CrossRef]

9. Karagiannidis, P.G.; Hodge, S.A.; Lombardi, L.; Tomarchio, F.; Decorde, N.; Milana, S.; Goykhman, I.; Su, Y.; Mesite, S.V.; Johnstone, D.N.; et al. Microfluidization of Graphite and Formulation of Graphene-Based Conductive Inks. *ACS Nano* **2017**, *11*, 2742–2755. [CrossRef]

10. Zhu, H.; Cao, Y.; Zhang, J.; Zhang, W.; Xu, Y.; Guo, J.; Yang, W.; Liu, J. One-step preparation of graphene nanosheets via ball milling of graphite and the application in lithium-ion batteries. *J. Mater. Sci.* **2016**, *51*, 3675–3683. [CrossRef]

11. Natarajan, C.; Fujimoto, H.; Mabuchi, A.; Tokumitsu, K.; Kasuh, T. Effect of mechanical milling of graphite powder on lithium intercalation properties. *J. Power Sources* **2001**, *92*, 187–192. [CrossRef]

12. Janowska, I.; Vigneron, F.; Bégin, D.; Ersen, O.; Bernhardt, P.; Romero, T.; Ledoux, M.J.; Pham-Huu, C. Mechanical thinning to make few-layer graphene from pencil lead. *Carbon* **2012**, *50*, 2679–3120. [CrossRef]

13. Moldovan, S.; Bulou, H.; Dappe, Y.J.; Janowska, I.; Bégin, D.; Pham-Huu, C.; Ersen, O. On the Evolution of Pt Nanoparticles on Few-Layer Graphene Supports in the High-Temperature Range. *J. Phys. Chem. C* **2012**, *116*, 9274–9282. [CrossRef]

14. Janowska, I. Evaporation-induced self-assembling of few-layer graphene into a fractal-like conductive macro-network with a reduction of percolation threshold. *Phys. Chem. Chem. Phys.* **2015**, *17*, 7634–7638. [CrossRef]

15. Blyth, R.I.R.; Buqa, H.; Netzer, F.P.; Ramsey, M.G.; Besenhard, J.O.; Golob, P.; Winter, M. XPS studies of graphite electrode materials for lithium ion batteries. *Appl. Surf. Sci.* **2000**, *167*, 99–106. [CrossRef]

16. Ferrari, A.C.; Meyer, J.C.; Scardaci, V.; Casiraghi, C.; Lazzeri, M.; Mauri, F.; Piscanec, S.; Jiang, D.; Novoselov, K.S.; Roth, S.; et al. Raman Spectrum of Graphene and Graphene Layers. *Phys. Rev. Lett.* **2006**, *97*, 187401. [CrossRef] [PubMed]

17. Paszkiewicz, S.; Janowska, I.; Pawlikowska, D.; Szymczyk, A.; Irska, I.; Lisiecki, S.; Stanik, R.; Gude, M.; Piesowicz, E. New functional nanocomposites based on poly(trimethylene 2,5-furanoate) and few layer graphene prepared by *in situ* polymerization. *Express Polym. Lett.* **2018**, *12*, 530–542. [CrossRef]

18. Eigler, S. A new parameter based on graphene for characterizing transparent, conductive materials. *Carbon* **2009**, *47*, 2933–2939. [CrossRef]

19. Pirzado, A.A.; Jouane, Y.; Le Normand, F.; Akilimali, R.; Papaefthimiou, V.; Matei Ghimbeu, C.; Janowska, I. Electrical Transport in "Few-Layer Graphene" Film Prepared by the Hot-Spray Technique: The Effect of Thermal Treatment. *J. Phys. Chem. C* **2014**, *118*, 873–880. [CrossRef]

20. Gutierrez, G.; Le Normand, F.; Muller, D.; Aweke, F.; Speisser, C.; Antoni, F.; Le Gall, Y.; Lee, C.S.; Cojocaru, C.S. Multi-layer graphene obtained by high temperature carbon implantation into nickel films. *Carbon* **2014**, *66*, 1–10. [CrossRef]

21. Yu, Y.-J.; Zhao, Y.; Ryu, S.; Brus, L.E.; Kim, K.S.; Kim, P. Tuning the Graphene Work Function by Electric Field Effect. *Nano Lett.* **2009**, *9*, 3430–3434. [CrossRef] [PubMed]

22. Tao, L.; Wang, Q.; Dou, S.; Ma, Z.; Huo, J.; Wang, S.; Dai, L. Edge-rich and dopant-free graphene as a highly efficient metal-free electrocatalyst for the oxygen reduction reaction. *Chem. Commun.* **2016**, *52*, 2764–2767. [CrossRef] [PubMed]

23. Kim, Y.J.; Yang, C.-M.; Park, K.C.; Kaneko, K.; Kim, Y.A.; Noguchi, M.; Fujino, T.; Oyama, S.; Endo, M. Edge-Enriched, Porous Carbon-Based, High Energy Density Supercapacitors for Hybrid Electric Vehicles. *ChemSusChem* **2012**, *5*, 535–541. [CrossRef] [PubMed]